World Conference on Timber Engineering Oslo 2023

LOCAL DAMAGE ASSESSMENT STRATEGY OF A TWO-STORY CLT WALL THROUGH VIBRATION-BASED NON-DESTRUCTIVE TECHNIQUES

Alexander Opazo-Vega[1], Franco Benedetti[2], Alan Jara-Cisterna[3], Peter Dechent[4]

ABSTRACT: This paper presents a methodology to evaluate the damage in CLT walls by applying non-destructive vibration-based methods. The main contribution is that the methodology allows locating the damage and estimating the severity of damage in the different wall joints, going beyond the typical global damage detections. One of the relevant aspects was the novel combination of Operational Modal Analysis, Finite Element Model Updating, and Regional Sensitivity Analysis. The methodology was successfully applied to a 2-story CLT module built in the laboratory and instrumented with accelerometers. The wall was evaluated in 11 different damage scenarios induced by incremental pseudo-static lateral loads. The results obtained correlated reasonably well with the visually observed damage, so it is estimated that this methodology could be extended to more complex CLT wall configurations.

KEYWORDS: Massive timber, CLT joint damage, Operational Modal Analysis, Model Updating, Sensitivity Analysis.

1 INTRODUCTION

Previous research has shown that earthquake-induced damage tends to be concentrated in the joints of CLT walls [1]. Therefore, it is desirable to assess the condition of these joints after seismic events. However, such an assessment cannot always be made visually because the joints are usually hidden behind non-structural elements.

To face the difficulties mentioned above, some researchers have preferred to instrument this type of buildings with sensors that measure the structural dynamic response induced by ambient or forced vibrations [2-5]. In this way, any relevant change in the measured dynamic properties can be an indicator of damage in its joints and thus justify a complete inspection. The dynamic properties most used as an indicator of damage in CLT buildings have been the natural vibration frequencies. For example, previous investigations have shown that the lateral frequencies can decrease between 15% and 36% depending on the level of lateral solicitation [6-10]. However, these investigations have only focused on detecting global damage without providing information about the localization of the damage in the joints or the associated level of local damage severity.

This work aims to propose a methodology to detect, locate, and evaluate the severity of damage in CLT wall joints. The methodology mentioned above combines Operational Modal Analysis (OMA), Finite Element Model Updating (FEMUP), and Regional Sensitivity Analysis (RSA), applied to a two-story CLT wall of cross-section H. The results obtained are expected to contribute to structural health monitoring of two-story CLT dwellings in developing countries.

2 MATERIAL AND METHODS

2.1 DESCRIPTION OF THE CLT WALL

One 2.6-m-long, 1.2-m-wide, and 4.2-m-high CLT wall was built from the assembly of eight wall panels (2.0-m-high, 1.2-m-wide) and two slab panels (2.6-m-long, 1.2-m-wide) (Figure 1). All CLT panels had a thickness of 100 mm consisting of three layers of C16 Radiata Pine timber bonded with bi-component polyurethane.

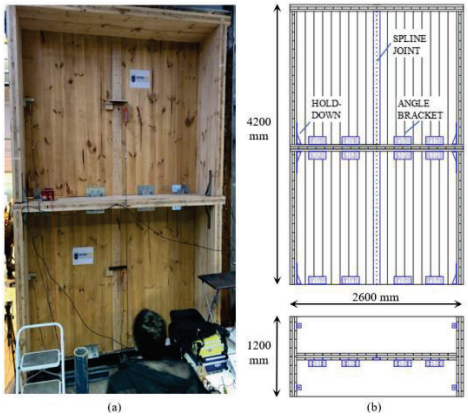

Figure 1: *(a)Laboratory assembly, (b)Dimensions and joints.*

[1] Alexander Opazo-Vega, University of Bío-Bío, Chile, aopazove@ubiobio.cl
Centro Nacional de Excelencia para la Industria de la Madera (CENAMAD), Pontificia Universidad Católica de Chile.
[2] Franco Benedetti, University of Bío-Bío, Chile, fbenedet@ubiobio.cl
Centro Nacional de Excelencia para la Industria de la Madera (CENAMAD), Pontificia Universidad Católica de Chile.
[3] Alan Jara-Cisterna, University of Bío-Bío, Chile, afjara@ubiobio.cl
[4] Peter Dechent, University of Concepción, Chile, pdechen@udec.cl

https://doi.org/10.52202/069179-0258

The CLT panels were joined together through metal hardware, screws, and nails. To prevent the panels from uplifting, metal hardware of the hold-down type (model HTT4) was used. On the other hand, metal hardware of the angle brackets type (model ABR255) was used to avoid the relative horizontal sliding of the panels. Furthermore, the hold-down and angle brackets used ring-shank nails (CNA 4x60mm) and bolts (diameter 13mm) to connect to the different panels. Finally, to avoid relative vertical slippage between panels, spline-type joints were used, with pieces of wood screwed to the panels (2 DSVT3R screws spaced every 100mm). All the connector models mentioned above are shown in Figure 2, while their quantity and distribution are shown in Table 1.

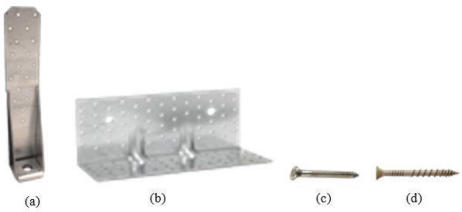

Figure 2:*(a) HTT4 hold-down, (b) ABR255 angle bracket, (c) CNA 4.0x60 nail (HTT4, ABR255), (d) DSVT3R screw (spline joints)*

Table 1: *Quantity and distribution of connectors*

Item	Story 1	Story 2
Number of hold-downs (number of nails)	8(18)	4(9)
Number of angle brackets (number of nails)	8(40)	4(35)
Number of screws in vertical spline joints	2@100mm	2@100mm

2.2 METHODOLOGY FOR ESTIMATING DAMAGE LOCATION AND SEVERITY

The proposed methodology has four stages: 1) induction of initial global damage, 2) measurement of dynamic properties, 3) numerical model simulations, and 4) regional sensitivity analysis.

2.2.1 Induction of initial global damage

In the first stage, initial damage is induced in the structure by applying a pseudo-static lateral load on the second story. The load is applied in the longitudinal direction X, parallel to the web panels, as shown in Figure 3. After maintaining the load for a few minutes, the wall is completely unloaded. This first stage was carried out 11 times with different levels of initial loads to generate different levels of damage to the walls. The first time this stage was performed, a minimal lateral load was applied, close to 0 kN, to adjust the measurement systems. On the other hand, in the following ten times, the lateral loads were increased every 10 kN until reaching 100 kN.

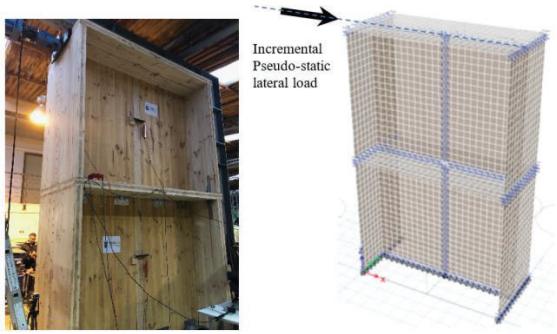

Figure 3: *Incremental pseudo-static test.*

2.2.2 Measurement of dynamic properties

Then, in the second stage, the dynamic properties of the wall (frequencies and modal shapes) are measured using OMA techniques (EFDD and SSI methods) [11]. The wall is excited through a series of low-energy impacts in the X direction. The impacts are applied at the intersection between the left flange panel and the web wall panel but at different heights. On the other hand, the lateral dynamic response is recorded in the right flange panel through six uniaxial accelerometers oriented in the X direction. With this information, it is possible to identify the first two frequencies and modal shapes in the X direction of the wall. It is important to note that this stage is also performed 11 times immediately following each load-unload level applied in the first stage. The experimental setup mentioned above is shown in Figure 4.

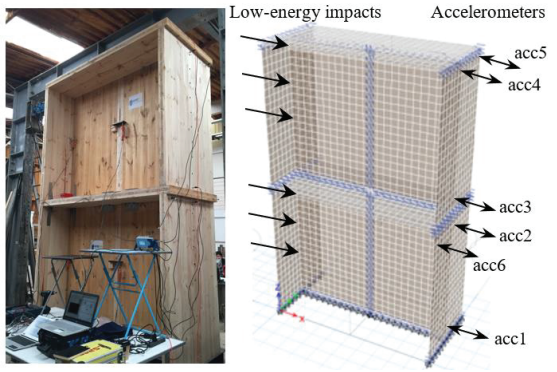

Figure 4: *Dynamic impact testing.*

2.2.3 Numerical model simulations

Next, in the third stage, a 3D finite element model of the wall is generated in the ETABS software to calculate its dynamic properties numerically. The CLT panels were modeled with four-node linear-elastic orthotropic shell elements. Their elastic properties were obtained from previous investigations [12]. On the other hand, the most relevant connections were modeled through link-type elements with uniaxial multilinear-elastic properties, as

https://doi.org/10.52202/069179-0258

shown in Figure 5. In the numerical model, it was assumed that the hold-down connectors only restrict displacements in the vertical direction to avoid the uplift of the wall panels (HD_1 to HD_4). On the other hand, for the angle-bracket connectors, it was assumed that they could restrain both vertical (AB_{t1} to AB_{t8}) and horizontal (AB_{s1} to AB_{s8}) displacements, but in an uncoupled manner. Finally, for the spline connectors, it was assumed that they could only restrain relative vertical displacements between the central wall panels. Therefore, the model considered 22 link-type elements to incorporate the relevant degrees of freedom of the connectors.

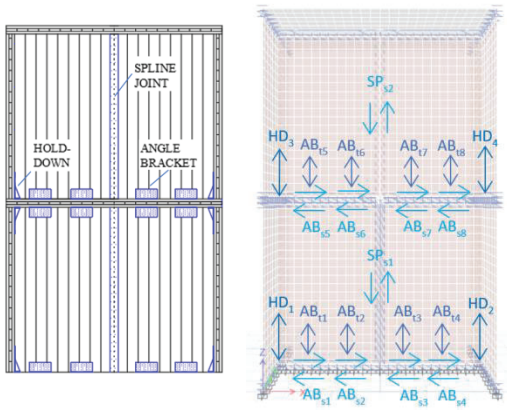

Figure 5: *Numerical model and input parameters.*

Each of the link-type elements of the model was assigned a multilinear-elastic force-deformation curve in their respective degrees of freedom. Specifically, a tri-linear axial force-deformation curve in tension and a linear force-deformation curve in compression were assigned to HD and AB's vertical degrees of freedom (see Figure 6a). These differences in the tensile and compressive behaviors are because these connectors are only susceptible to damage and stiffness degradation in the vertical direction when tensile. At the same time, when compressed, they maintain a high stiffness that is controlled by the crushing in the CLT panels. On the other hand, trilinear-elastic force-deformation curves were assigned to the ABs in the horizontal direction and to the SPs in the vertical direction because in those degrees of freedom, the aforementioned connectors work in shear (see Figure 6b).

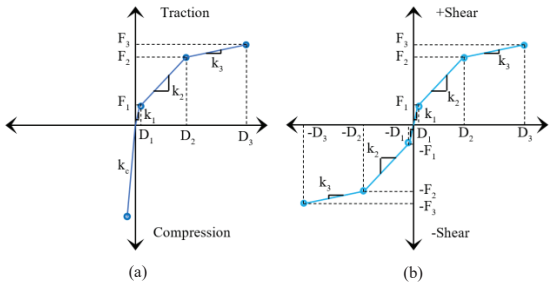

Figure 6: *Force-deformation curves: (a) tension, (b) shear.*

As can be seen in Figure 6, several input parameters are needed to define the force-deformation curves in multilinear-elastic link elements. However, several of these parameters were assumed as constants to simplify the model, considering results from previous experimental tests on similar connectors. For example, the first section of the tri-linear curves mainly represents the joints' friction mechanisms. In that section, the value of D_1 is small and quite close to 0.5 mm. Moreover, the stiffness k_1 of that section is generally very high and four times the stiffness of the second section k_2. The second section is one of the most important since it represents the elastic stiffness of the connectors, which the manufacturers generally report in their catalogs. Finally, the third section represents the degradation of the elastic stiffness of the connector, with deformation values ranging from D_2=4mm to D_3=15mm on average and a stiffness k_3 of the order of half of k_2. Therefore, given the importance of the parameter k_2, it will be assumed as the only input variable and indicator of the eventual damage to each of the connectors. The rest of the parameters will be assumed as constant or as a function of k_2 (D_1=0.5mm, D_2=4mm, D_3=15mm, k_1/k_2=4, k_3/k_2=0.5).

Once the finite element model is defined, running a series of numerical simulations is possible. Each numerical simulation has a different set of values of its 22 relevant input parameters, i.e., the k_2 elastic stiffnesses of the AB, HD, and SP connections. In this way, it is possible to calculate a set of dynamic properties of the wall in each numerical simulation through the solution of a finite element eigenvalue and eigenvector problem. These "simulated" dynamic properties of the wall correspond to the output parameters of the model.

It is essential to consider the possible combinations of the 22 input parameters of the model in the best way. For this purpose, a minimum and maximum value of k_2 must first be defined for each type of connector, representing different levels of damage, from severe to minor, respectively. The values considered are shown in Table 2 and were obtained from previous research [13]. Then, for each k_2 range, 2400 values are sampled with the Latin hypercube technique, assuming a uniform distribution and varying all input parameters at the same time. The execution of the numerical simulations was done by combining the API tools of the ETABS finite element software and the Python programming language.

Table 2: *Minimum and maximum values for k_2 joint stiffnesses.*

Item	Min (kN/mm)	Max (kN/mm)
HD_1 to HD_4	0.18	7.15
AB_{t1} to AB_{t8}	0.15	9.20
AB_{s1} to AB_{s8}	0.94	14.00
SP_{s1} to SP_{s2}	0.02	0.81

2.2.4 Regional sensitivity analysis

Finally, in the fourth stage, a regional sensitivity analysis (RSA) [14] is applied to each of the 11 damage levels induced to the wall in stage one. The objective of RSA is

https://doi.org/10.52202/069179-0258

to identify which joint stiffnesses (22 input parameters) are most influential on the dynamic properties of the wall and in what range of values these stiffnesses are most influential.

A necessary first step in applying RSA is to define an objective function (defined Y), which is an estimation of model performance calculated by comparison of measured and simulated variables. In the context of this work, it is convenient to choose the objective function as the differences between the dynamic properties measured in the wall (step two) and the dynamic properties simulated in the models (step three). Furthermore, as the simulated dynamic properties depend on the input parameters (stiffnesses of the joints stored in a vector k), the objective functions also depend on these input parameters ($Y_{(k)}$).

The dynamic properties are sometimes scalar (vibration frequencies) and sometimes vectors (modal shapes); therefore, it is advisable to use an objective function that includes both kinds of dynamic properties. Accordingly, Equation 1 shows the expression of $Y_{(k)}$.

$$Y_{(k)} = \alpha \cdot \frac{1}{n}\sum_{i=1}^{n}\left|\frac{\tilde{f}_i - f_{i(k)}}{\tilde{f}_i}\right| + \beta \cdot \frac{1}{n}\sum_{i=1}^{n} NMD\left(\tilde{\phi}_i, \phi_{i(k)}\right) \quad (1)$$

where n is the number of identified dynamic properties (two in this case), $\tilde{f}_i$ are the measured frequencies, $f_{i(k)}$ are the simulated frequencies, NMD is the normalized modal difference [11], $\tilde{\phi}_i$ are the measured modal shape vectors, and $\phi_{i(k)}$ are the simulated modal shape vectors. The α and β constants take values between 0 and 1 depending on the relative importance to be given to the differences between frequencies concerning the differences between modal forms. In this case, both were assumed to be equal to 0.5.

After defining the objective functions, RSA requires that the models be separated into two groups. The first group corresponds to all models with objective function values below a specific acceptable threshold. These models are generally referred to as behavioral (B models) and, in this case, are characterized by generating simulated dynamic properties that differ very little from the measured dynamic properties. On the other hand, the rest of the models, which have objective function values higher than the threshold, are called non-behavioral models (NB models). Consequently, the acceptable threshold value was selected as 0.15 for the objective function $Y_{(k)}$.

Once it is known which models belong to groups B and NB, RSA requires the calculation of the cumulative density functions (CDF) of each input parameter for both B and NB models. That information makes it possible to rank which input parameters influence the objective functions most. For example, if, for an input parameter, the CDF of the B models is different from the CDF of the NB models, then that input parameter is very influential on the objective functions. However, this degree of influence is only sometimes possible to distinguish graphically; therefore, it is usual to resort to the Kolmogorov-Smirnov (K-S) statistical test to estimate the degree of influence of the input parameter. According to the suggestions of [13], an input parameter can be grouped into three possible sensitivity classes depending on the p-value obtained in the K-S test: critical (p-value < 0.01), important (0.01< p-value < 0.1), and negligible (p-value > 0.1). This kind of ranking of the influence of the input parameters helps estimate the location of the joints that could suffer more damage, given a variation in the global dynamic properties of the wall.

Finally, with the data associated with the B models, it is possible to know in what range of values the input parameters most influenced the objective functions. These ranges can be quickly visualized through box plots of the input parameters and further analyzed using the ANOVA statistical test. In this way, it is possible to evaluate the severity of the damage in the joints by studying the variation of their stiffnesses.

3 RESULTS AND DISCUSSION

3.1.1 Variation of the wall's dynamic properties

Figure 7 shows the variation of the first two vibration frequencies measured in the wall as the lateral load increased and, therefore, the level of damage. On the other hand, Figure 8 shows the modal shapes measured in the right-flange wall.

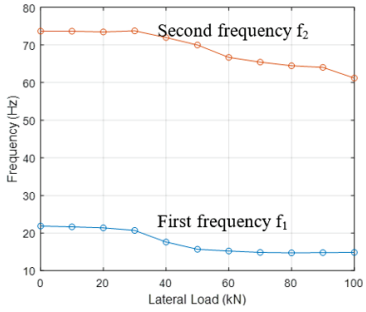

Figure 7: *Measured vibration frequencies.*

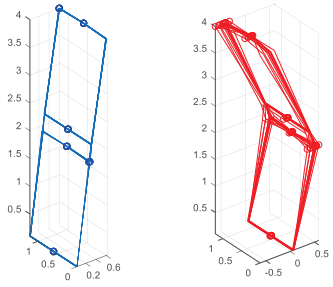

Figure 8: *Measured modal shapes: first vibration mode (left), second vibration mode (right).*

Figure 7 shows that the two vibration frequencies identified were decreasing as the damage caused by lateral loads increased. The decreases of the frequencies between

the undamaged and maximum damage states were 32% and 17% for f_1 and f_2, respectively. These decreases are the first global indicator of damage in the CLT wall joints; however, they do not indicate where the damage may be located or the severity of the joints' stiffness degradation. The measured modal shapes shown in Figure 8 suggest that the first vibration mode experienced almost no variation in the different levels of damage induced. However, the second mode of vibration showed more relevant variations as the lateral load on the wall increased.

3.1.2 Damage location and severity estimation.

The first relevant result of the RSA was ranking the most influential joint rigidities in the *Y* function. At each lateral load level, the value of *Y* was calculated for each simulated combination of input parameters and compared with the threshold value of 0.15. In this way, it was possible to separate the B models from the NB models and to visualize these results in scatter plots and CDF curves. Some examples of the graphs mentioned above are shown in Figures 9 to 12.

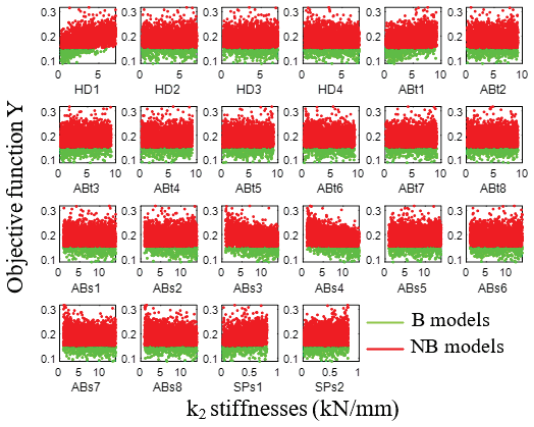

Figure 9: *Dispersion plots for k_2 stiffnesses, after 50kN lateral load.*

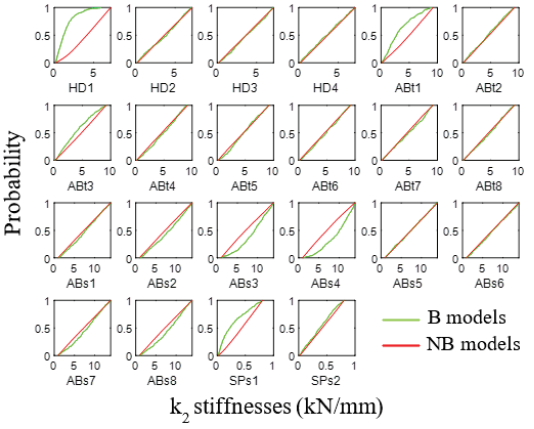

Figure 10: *CDF curves for k_2 stiffnesses, after 50kN lateral load.*

Then, applying the K-S test to the CDF curves, it was possible to obtain the ranking of the most influential stiffnesses of the connectors. Table 3 shows the top 5 ranking for each lateral load level.

Table 3: *Ranking of the most influential k_2 stiffnesses.*

Lateral Load (kN)	1st	2nd	3rd	4th	5th
0	AB_{s4}	AB_{s3}	HD_1	AB_{s8}	AB_{s7}
10	AB_{s4}	AB_{s3}	HD_1	AB_{s8}	AB_{s7}
20	AB_{s4}	AB_{s3}	HD_1	AB_{s8}	AB_{s7}
30	AB_{s4}	AB_{s3}	HD_1	AB_{s8}	AB_{s7}
40	AB_{s4}	AB_{s3}	HD_1	SP_{s1}	AB_{s2}
50	HD_1	AB_{t1}	SP_{s1}	AB_{s4}	AB_{s3}
60	HD_1	AB_{t1}	AB_{s3}	SP_{s1}	AB_{s4}
70	HD_1	AB_{t1}	SP_{s1}	AB_{s3}	SP_{s2}
80	HD_1	AB_{t1}	SP_{s1}	AB_{s4}	AB_{s3}
90	HD_1	AB_{t1}	SP_{s2}	SP_{s1}	AB_{s3}
100	HD_1	SP_{s2}	AB_{t1}	HD_3	SP_{s1}

From Table 3, up to the lateral load of 40kN, the most influential connectors were the angle brackets working in shear on the right side of the wall on the first and second floors (AB_{s4}, AB_{s3}, AB_{s8}, and AB_{s7}). Exceptionally, the tension stiffness of the hold-down on the left side of the first floor (HD_1) also appeared. These results are reasonable since there was practically no damage to the connectors for lateral loads less than 40kN, and most of the deformation was associated with the relative horizontal sliding of the wall panels. However, from a lateral load of 50kN onwards, the influence ranking of the connectors changed radically. The level of damage to the connectors increased, and the deformation mechanisms were those associated with wall rocking. Therefore, the tension stiffness of HD_1, the tension stiffness of AB_{t1}, and the vertical shear stiffness of SP_{s1} took an important role in the first story of the wall. This can also be seen in Figures 9 and 10. For a lateral load of 50kN, the B models tend to concentrate on the lower values of the stiffnesses of HD_1, AB_{t1}, and SP_{s1}, with more severe damage levels expected in these zones. The severity of damage in these connectors can be analyzed by studying the evolution of their stiffnesses in the B models for different lateral load levels. Figures 11 to 13 show this through box plots.

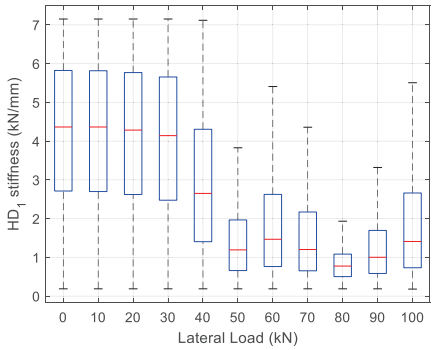

Figure 11: *Boxplot of k_2 stiffnesses for HD_1 connector.*

https://doi.org/10.52202/069179-0258

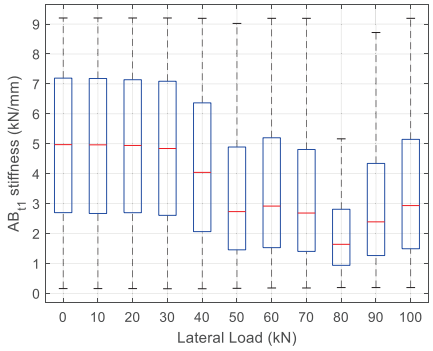

Figure 12: *Boxplot of k_2 stiffnesses for AB_{t1} connector.*

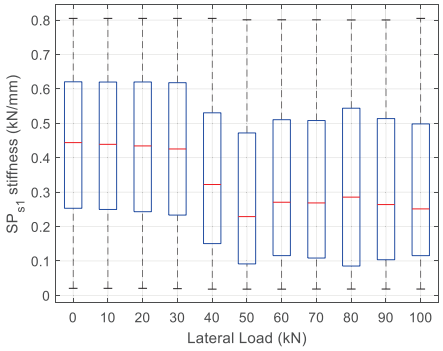

Figure 13: *Boxplot of k_2 stiffnesses for SP_{s1} connector.*

Figures 11 to 13 show that significant degradation of the stiffness of HD_1, AB_{t1}, and SP_{s1} connectors occurred as the lateral load increased. The initial stiffnesses of these connectors decreased by 63%, 36%, and 27%, respectively. These stiffness reductions obtained by the proposed vibration-based non-destructive method closely matched the real damage observed, as shown in Figures 14 to 16 [].

Figure 14: *Damage in HD_1 connector after 100kN lateral load.*

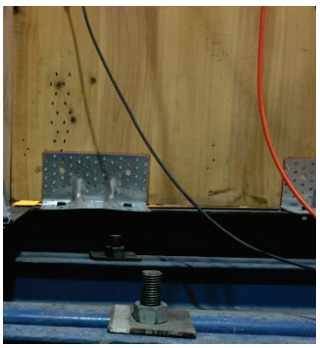

Figure 15: *Damage in AB_{t1} connector after 100kN lateral load.*

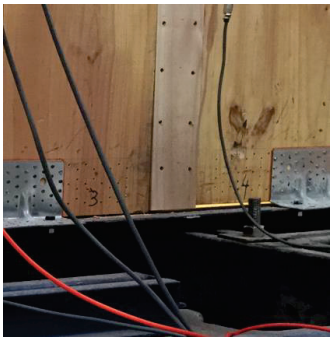

Figure 16: *Damage in SP_{s1} connector after 100kN lateral load.*

4 CONCLUSIONS

In this paper, we have described a new approach to estimate the location and severity of damage in CLT wall joints based on OMA, FEMUP and RSA techniques. We have obtained satisfactory results showing that this non-destructive methodology can be extended to more complicated structural configurations.

REFERENCES

[1] M. Izzi, D. Casagrande, S. Bezzi, D. Pasca, M. Follesa, R. Tomasi.: Seismic behaviour of Cross-Laminated Timber structures: A state-of-the-art review. Engineering Structures, 170: 42–52, 2018.

[2] T. Reynolds, R. Harris, W.-S. Chang, J. Bregulla, & J. Bawcombe.: Ambient vibration tests of a cross-laminated timber building. Proceedings of the Institution of Civil Engineers - Construction Materials, 168(3): 121-131, 2015.

[3] T. Reynolds, D. Casagrande, & R. Tomasi.: Comparison of multi-storey cross-laminated timber and timber frame buildings by in situ modal analysis. Construction and Building Materials, 102: 1009-101, 2016.

[4] A. Aloisio, D. Pasca, R. Tomasi, & M. Fragiacomo.: Dynamic identification and model updating of an eight-storey CLT building. Engineering Structures, 213: 110593, 2020.

[5] B. Kurent, B. Brank, & W. K. Ao.: Model updating of seven-storey cross-laminated timber building designed on frequency-response-functions-based modal testing. Structure and Infrastructure Engineering, 0(0): 1-19, 2021.

[6] A. Ceccotti, C. Sandhaas, M. Okabe, M. Yasumura, C. Minowa, & N. Kawai.: SOFIE project – 3D shaking table test on a seven-storey full-scale cross-laminated timber building. Earthquake Engineering & Structural Dynamics, 42(13): 2003-2021, 2013.
[7] G. Flatscher, & G. Schickhofer.: Shaking-table test of a cross-laminated timber structure. Proceedings of the Institution of Civil Engineers - Structures and Buildings, 168(11): 878-888, 2015.
[8] M. Popovski, & I.Gavric.: Performance of a 2-Story CLT House Subjected to Lateral Loads. Journal of Structural Engineering, 142(4): E4015006, 2016.
[9] F. T. Matos, J. M. Branco, P. Rocha, T. Demschner, & P. B. Lourenço.: Quasi-static tests on a two-story CLT building. Engineering Structures, 201: 109806, 2019.
[10] I. Mugabo, A. R. Barbosa, A. Sinha, C. Higgins, M. Riggio, S. Pei, J. W. van de Lindt, & J. W. Berman.: System Identification of UCSD-NHERI Shake-Table Test of Two-Story Structure with Cross-Laminated Timber Rocking Walls. Journal of Structural Engineering, 147(4): 04021018, 2021.
[11] C. Rainieri, G. Fabbrocino.: Operational Modal Analysis of Civil Engineering Structures. Springer New York, 2014.
[12] A. Opazo-Vega, F. Benedetti, M. Nuñez-Decap, N. Maureira-Carsalade, & C. Oyarzo-Vera.: Non-Destructive Assessment of the Elastic Properties of Low-Grade CLT Panels. Forests, 12(12): 1734, 2021.
[13] F. Benedetti, V. Rosales, A. Opazo-Vega, S. Sepulveda, A. Jara-Cisterna.: Experimental analysis of a two-story three dimensional panelized CLT module. In: Proceedings of the World Conference on Timber Engineering, Chile, 2021.
[14] A. Saltelli, M. Ratto, T. Andres, F. Campolongo, J . Cariboni, D. Gatelli, M. Saisana, S. Tarantola.: Global sensitivity analysis: the primer. John Wiley & Sons, 2008.

https://doi.org/10.52202/069179-0258